

Confirmation of sub-solar metallicity for WASP-77Ab from JWST thermal emission spectroscopy

PRUNE C. AUGUST ^{1,2} JACOB L. BEAN ¹ MICHAEL ZHANG,^{1,*} JONATHAN LUNINE,³ QIAO XUE ¹,
MICHAEL LINE,⁴ AND PETER C. B. SMITH ⁴

¹*Department of Astronomy & Astrophysics, University of Chicago, Chicago, IL, USA*

²*Institute of Physics, École polytechnique fédérale de Lausanne (EPFL) Lausanne, Switzerland*

³*Department of Astronomy, Cornell University, Ithaca, NY, USA*

⁴*School of Earth and Space Exploration, Arizona State University, Tempe, AZ, USA*

ABSTRACT

We present the dayside thermal emission spectrum of WASP-77Ab from 2.8 – 5.2 μm as observed with the NIRSpec instrument on the James Webb Space Telescope (JWST). WASP-77Ab was previously found to have a sub-solar metallicity and a solar carbon-to-oxygen (C/O) ratio from H₂O and CO absorption lines detected using high-resolution spectroscopy. By performing atmospheric retrievals on the JWST spectrum assuming chemical equilibrium, we find a sub-solar metallicity $[\text{M}/\text{H}] = -0.91^{+0.24}_{-0.16}$ and C/O ratio $0.36^{+0.10}_{-0.09}$. We identify H₂O and CO and constrain their abundances, and we find no CO₂ in the spectrum. The JWST and high-resolution spectroscopy results agree within $\sim 1\sigma$ for the metallicity and within 1.8σ for the C/O ratio. However, our results fit less well in the picture painted by the shorter wavelength spectrum measured by HST WFC3. Comparing the JWST thermal emission spectra of WASP-77Ab and HD 149026b shows that both hot Jupiters have nearly identical brightness temperatures in the near-infrared, but distinctly different atmospheric compositions. Our results reaffirm high-resolution spectroscopy as a powerful and reliable method to measure molecular abundances. Our results also highlight the incredible diversity of hot Jupiter atmospheric compositions.

Keywords: Exoplanets(498) — Exoplanet atmospheres(487) — James Webb Space Telescope(2291)

1. INTRODUCTION

Atmospheric metallicity and carbon-to-oxygen (C/O) ratio are now well-established tracers for exoplanet characterisation (Madhusudhan 2012; Fortney et al. 2013; Venturini et al. 2016). In particular, their relevance regarding planetary formation processes has

been widely discussed in the literature (Pollack et al. 1996; Mordasini et al. 2016; Madhusudhan 2019). The James Webb Space Telescope (JWST) marks an important step in the field because it has the sensitivity to obtain high precision data over a broad range of wavelengths for a wide range of exoplanets, and therefore allows for strong and reliable constraints on these key markers (Greene et al. 2016).

* 51 Pegasi b Fellow

Hot Jupiters are giant gaseous bodies transiting very close to their host stars. These highly irradiated planets are unlike any of our Solar System planets, and questions like their origins, as well as how they tie into a bigger picture of planet formation, still remain largely unanswered (Fortney et al. 2021). Together with their obvious observational advantages, they thus make excellent candidates for transit spectroscopy and specifically atmospheric characterisation.

WASP-77Ab (Maxted et al. 2013) is a great target for such endeavours: this hot Jupiter is one of the highest signal-to-noise (S/N) planets for thermal emission measurements in the near-infrared (Kempton et al. 2018)¹. In a breakthrough result, observations using ground-based high-resolution spectroscopy (HRS) with the Immersion GRating INfrared Spectrometer (IGRINS) constrained the metallicity to be solar and C/O ratio to be solar based on the detection of H₂O and CO lines (Line et al. 2021).

Subsequent Hubble and Spitzer Space Telescope data confirmed the presence of water vapour on WASP-77Ab’s dayside (Mansfield et al. 2022), which indicates C/O values < 1 (Kreidberg et al. 2015; Benneke 2015). However, there are lingering questions about the composition of the planet because the Hubble data had some systematic outliers that couldn’t be fit by 1D models and because the retrieved metallicities differed somewhat (albeit only at the 1.8 σ confidence level), with Mansfield et al. (2022) estimating a solar to potentially 3x super-solar metallicity.

The low metallicity for WASP-77Ab inferred by Line et al. (2021) is surprising from an origins standpoint because gas giants are expected to accrete planetesimals that pollute their grow-

ing atmospheres during formation. Nevertheless, recent work suggests that subsolar atmospheric abundances for close-in giant planets indicates formation beyond the CO₂ snowline ($a > 5$ au, Bitsch et al. 2022). The results for WASP-77Ab are also surprising given the recent series of strong CO₂ detections in hot Jupiter atmospheres that are indicative of enhanced atmospheric metallicities (JWST Transiting Exoplanet Community Early Release Science Team et al. 2023; Rustamkulov et al. 2023; Alderson et al. 2023; Bean et al. 2023). Because of this and the very different data processing and analysis needed for ground- vs. space-based data it is important to provide an independent and precise measurement of these quantities for WASP-77Ab.

In this article, we analyze the dayside emission spectrum of WASP-77Ab obtained using the NIRSpec instrument on JWST. NIRSpec is an ideal instrument for this project because its bandpass covers key carbon- and oxygen-bearing molecules like H₂O, CO, CO₂ and CH₄. NIRSpec is also well suited for studying WASP-77Ab because it has a slit (1.6''x 1.6'') that allows the rejection of contaminating light without requiring roll angle constraints. The diffraction-limited point spread function of NIRSpec is significantly smaller (FWHM \approx 0.17'') than the separation of the two stars (\sim 3'', Δ mag \sim 2; Maxted et al. 2013), ensuring minimal blending and allowing for precise characterization of WASP-77Ab. We infer fundamental diagnostics like the atmospheric metallicity and C/O ratio, as well as estimates of the thermal structure of the atmosphere and its chemistry. We place our results in the context of the previous estimates provided by Line et al. (2021) and Mansfield et al. (2022), and we provide support for HRS as a method to retrieve chemical abundance constraints.

We describe how we obtained WASP-77Ab’s dayside emission spectrum in Section 2, with a

¹ See tabulated values for known planets at the TESS Atmospheric Characterization Working Group webpage: <https://tess.mit.edu/science/tess-acwg/>.

focus on the partial phase curve detection. Section 3 is dedicated to the atmospheric retrievals and their results. We also provide a comparison with other data sets for WASP-77Ab. To further illustrate the diversity of hot Jupiters, we contrast WASP-77Ab with HD 149026b, observed in eclipse by JWST NIRCам (Bean et al. 2023), in Section 4. Finally, we summarize our results in Section 5.

2. OBSERVATIONS AND DATA REDUCTION

We observed a secondary eclipse of WASP-77Ab on August 24-25, 2022 between 22:12 - 04:36 UTC with JWST NIRSpec (program GTO 1274, J. Lunine PI). The observations used the Bright Object Time-Series (BOTS) mode, with the G395H grating and F290LP filter combination (Birkmann et al. 2022). The duration of this observation was 6.4 hours for a total of 1419 integrations, and 17 groups per integration. The observation began 2.44 hours before the secondary eclipse and continued for 1.80 hour after eclipse egress. The wavelength coverage for the two sensor chip assemblies (or detectors) used in this observation, NRS 1 and NRS 2, are $2.674 - 3.716 \mu\text{m}$ and $3.827 - 5.173 \mu\text{m}$ respectively. We used the SUB32 subarray and the NRSRAPID readout pattern.

We reduced the raw data using the **Eureka!** pipeline (Bell et al. 2022). This pipeline offers a reduction in 6 stages. The first two are essentially the same as the JWST Science Calibration Pipeline (`rwst`, Bushouse et al. 2023). The following three perform background subtraction and spectral extraction, spectroscopic light curve generation, and spectroscopic light curve fitting.

The system parameters used for the secondary eclipse are a planet orbital period $P = 1.3600309$ days, ratio of the planet’s semi-major axis to the host star radius $a/R_s = 5.43$, planetary orbital inclination $= 89.4^\circ$, and planetary orbital eccentricity $e = 0.0$ (Mansfield et al. 2022). Varying

these parameters within their uncertainties did not impact the results. The secondary eclipse times were estimated by fitting the white light curves created for each of the NIRSpec detectors, and then used for all spectroscopic light curves. A nested sampling algorithm was used for all the parameter estimation. The measured secondary eclipse time is consistent with a circular orbit within the uncertainties of the most recent ephemerides (Ivshina & Winn 2022; Kokori et al. 2022; Cortés-Zuleta et al. 2020). The bin size of these channels is set to 13/17nm for NRS1/2 in an effort to balance out precision and retrieval performances.

The data are processed into a final spectrum in Stage 6. We fine-tuned parameters such as the spectral and background aperture, outlier rejection, and binning in order to minimize the median absolute deviation of the final light curves and following the steps and recommendations of Alderson et al. (2023). We performed tests of varying the different reduction parameters (apertures, sigma clipping and outlier rejection thresholds, binning, etc) in order to assess their impact on the resulting spectrum. All of these showed minimal to no impact on the final spectrum, indicative of its robustness vis-à-vis the data reduction process.

Except for a constant rate linear trend in time, which is a standard feature of NIRSpec time-series data (Rustamkulov et al. 2023; Alderson et al. 2023; Mikal-Evans et al. 2023; Moran et al. 2023; Lustig-Yaeger et al. 2023), the light curves are largely unaffected by systematics. In particular, there is no exponential ramp in the first few hours of the observation as has been seen for other early JWST observations (Bean et al. 2023). We therefore analyzed the full time series without trimming any data from the start. The exceptional quality of the spectroscopic data combined with the short period of the target’s orbit raised the question of whether the phase curve of the planet could be detected

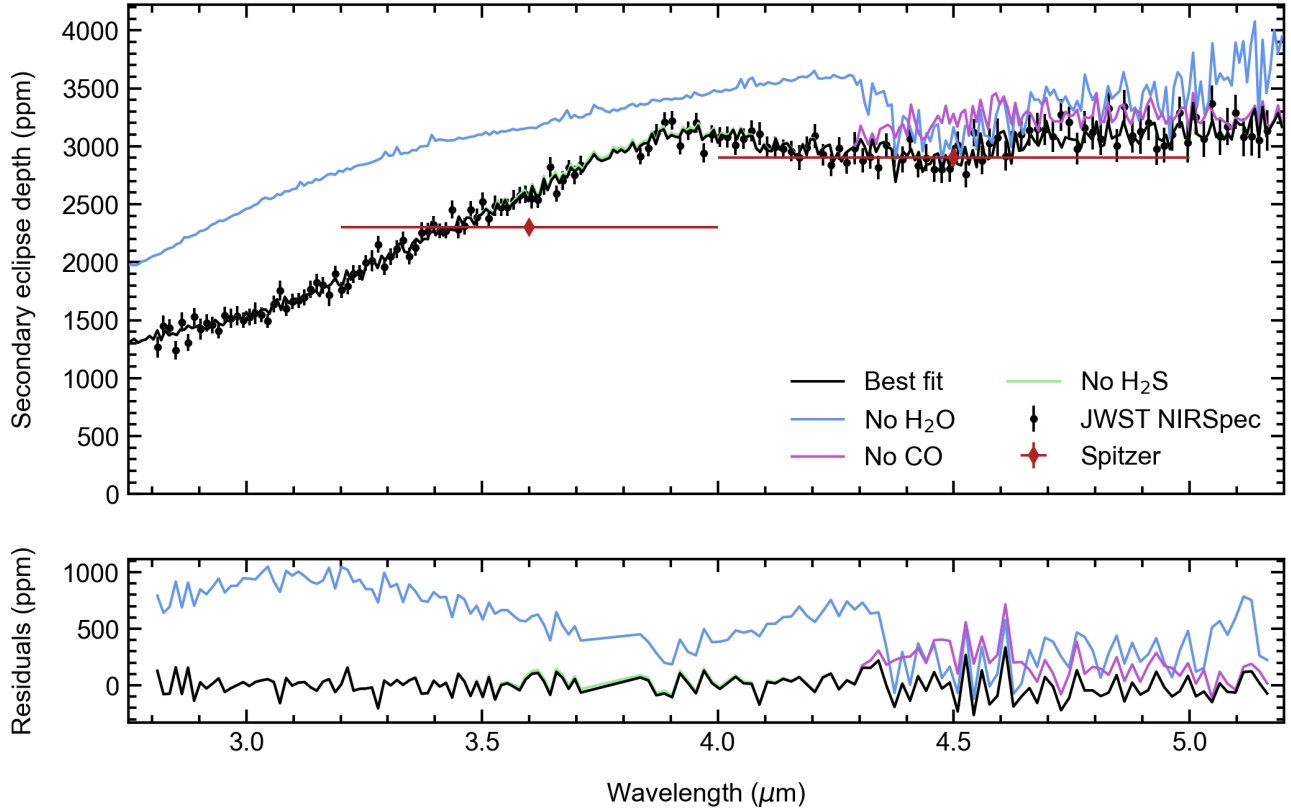


Figure 1. Thermal emission spectrum of WASP-77Ab as observed by JWST NIRSpec/G395H, along with the best fit model (black line). The different coloured lines correspond to best fit spectrum computations with different molecular opacities zeroed out. The bottom panel shows the residuals.

(e.g., [Coulombe et al. 2023](#)). In order to investigate this, a first order phase curve model (see Equation 1) was added to the spectroscopic light curve fitting.

$$f_{pc}(\phi) = 1 + A \cdot (\cos(\phi) - 1) + B \cdot \sin(\phi), \quad (1)$$

where $\phi = \frac{2\pi}{P}(t - t_{sec})$ and t_{sec} is the time of secondary eclipse.

The *Eureka!* partial phase curve fitting for the white light curves of each detector allowed us to retrieve relative amplitudes of $\tilde{a}_1 = 0.39 \pm 0.09$ and $\tilde{a}_2 = 0.42 \pm 0.11$. The estimated phase shifts in degrees read $\phi_1 = 18 \pm 10$ and $\phi_2 = 9 \pm 12$ respectively. Taking all the values estimated through fitting the spectroscopic light curves, we found an average relative amplitude of $\mu_a = 0.54$ ($\sigma_a = 0.17$) and an average phase shift of $\mu_\phi = 11^\circ$ ($\sigma_\phi = 35^\circ$). These results will be investigated further in a future paper looking

at both the phase curve and the eclipse mapping signals in the data.

While on such a short window the phase curve detection is not statistically significant, it is physically motivated. Overall, the phase curve fitting doesn't have a determining impact on the final shape of the spectrum beyond a small shift upwards of about $\simeq 100$ ppm. Higher order systematic models such as a quadratic polynomial in time have a similar effect.

The final resulting spectrum is shown in Figure 1, along with the Spitzer datapoints collected from [Mansfield et al. \(2022\)](#). Our spectrum agrees with these within 2σ for both the $3.6\mu\text{m}$ and the $4.5\mu\text{m}$ channels. The derived error inflation factor for the spectroscopic light curves is typically 1.5, and the typical RMS of the residuals is 230 ppm. From the modeling we find that we see broad absorption features

of H₂O and CO. The spectrum doesn't show any features corresponding to a CO₂ signature, nor do we see any emission features indicative of a thermal inversion.

3. RETRIEVALS

We performed retrievals using PLATON (Zhang et al. 2019; Zhang et al. 2020) with different temperature-pressure (TP) profile parametrizations and assumptions for the chemistry. We used the HELIOS-K (Malik et al. 2017a, 2019a) generated opacity files for the following molecules: CH₄, CO₂, CO, H₂O, H₂S, NH₃ and SO₂. We used the nested sampling algorithm, with 1,000 live points and R=20,000 opacity files. In addition to the retrieval setup and parameters already offered by PLATON for the thermal and chemical structure of the atmosphere, we implemented a dilution factor as described in Taylor et al. (2020) to account for inhomogeneities across the dayside while performing a 1-D retrieval. This parameter ranges from 0 to 1, with unity corresponding to a perfectly homogeneous dayside.

We used three models to describe the TP profile WASP-77Ab's atmosphere. The first is a version of the the analytic, level-by-level parameterization suggested by Guillot (2010), redefined by Line et al. (2013a) to include a second irradiation stream, and implemented in PLATON under the name "radiative solution". This model has five free parameters: thermal opacity κ , visible to thermal opacity ratio of the two streams included in the model, γ and γ_2 , the percentage α apportioned to the second stream, and the effective albedo β . The second type of TP profile we used is a parametric model established by Madhusudhan & Seager (2009). This model consists of placing three anchor points (P_i, T_i) and linking them to each other with exponential curves parameterized by α_i . Beyond and below the first and last anchor point, the profile is assumed to be isothermal. The prior ranges for this profile are approximately

the same as the ones used in Line et al. (2021) to allow for adequate comparison. Finally, the last TP profile is a similar "three layers" structure with lapse rates between them, which we refer to as the piece-wise solution. There are also 6 free parameters: three pressures P_i and three lapse rates k_i .

The chemical properties and composition of the atmosphere were probed using both equilibrium and free chemistry. For the free retrieval we modified PLATON to retrieve the abundances of five molecules (H₂O, CO, CO₂, CH₄, and H₂S). Their abundance profile was fixed to be constant with altitude and evaluated through a logarithmic prior ranging from $[-16, 0]$ in the free retrieval. The equilibrium chemistry is built into PLATON via GGChem (Woitke et al. 2018).

Out of all the model combinations tested for the retrieval, the best fit to the spectral data, obtained with a Line et al. (2013a) style TP profile and using equilibrium chemistry, is shown in Figure 1. It fits to the data with a reduced $\chi^2 = 0.78$ (150 data points and 8 free parameters), and has in particular $[M/H] = -0.97$, C/O = 0.33, a dilution factor 0.99, and the TP profile shown on the far left panel in Figure 2 (confidence intervals on the abundances are given below). The coloured lines in Figure 1 are the spectra computed when fixing the best fit values and zeroing the opacities of different molecules, effectively removing them from the radiative transfer but not changing the mean molecular weight of the atmosphere. The full data for this plot can be found in Table 2.

The TP profile is shown in the far left panel of Figure 2. In particular, the best fits estimated through three different models (Line et al. 2013a; Madhusudhan & Seager 2009, and the piece-wise solution) are plotted in black lines along with the 2σ confidence interval from the samples. These retrievals gave results for the composition of the atmosphere that were consistent within 1σ with the main results (us-

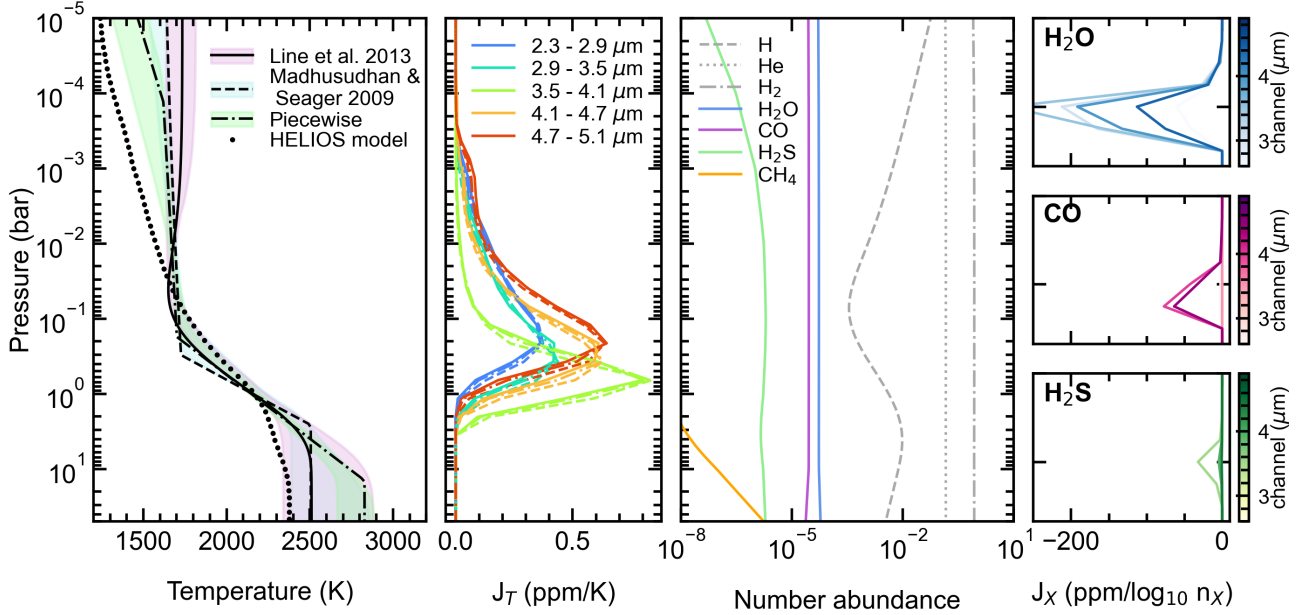


Figure 2. Description of the vertical atmospheric structure of WASP-77Ab’s dayside. On the left, the first and second panel show the thermal structure along with the temperature Jacobians, which characterize the spectrum’s sensitivity to small changes in the temperature. On the right, the third panel shows the chemical profiles and the three subplots investigate the abundance Jacobians of the main molecules we are sensitive to: H₂O, CO, and H₂S.

Data	TP model	[M/H]	[M/H] _{best}	C/O	C/O _{best}	χ^2_ν
JWST NIRSpec	L+13	$-0.91^{+0.24}_{-0.16}$	-0.97	$0.36^{+0.10}_{-0.09}$	0.33	0.778
	MS09	$-1.03^{+0.34}_{-0.18}$	-1.16	$0.29^{+0.11}_{-0.06}$	0.28	0.778
	Piece-wise	$-0.96^{+0.16}_{-0.12}$	-1.04	$0.31^{+0.07}_{-0.05}$	0.30	0.796
JWST NIRSpec + HST WFC3	L+13	$-0.06^{+0.13}_{-0.16}$	-0.00	$0.60^{+0.04}_{-0.05}$	0.61	1.163
	MS09	$-0.18^{+0.16}_{-0.15}$	-0.11	$0.47^{+0.07}_{-0.06}$	0.51	1.127
	Piece-wise	$-0.07^{+0.13}_{-0.17}$	-0.06	$0.52^{+0.05}_{-0.06}$	0.55	1.163

Table 1. Summary of the metallicity and carbon-to-oxygen ratio estimates assuming equilibrium chemistry and

different parameterizations for the TP profile, both with and without including the HST WFC3 data. “L+13” refers to [Line et al. \(2013a\)](#), “MS09” to [Madhusudhan & Seager \(2009\)](#) and the piece-wise model has been presented in [Section 3](#).

ing the profile from [Line et al. 2013a](#)) quoted here. The retrieval outcomes of these different models is found in [Table 1](#). We also compare to the TP profile calculated by HELIOS ([Malik et al. 2017b, 2019b](#)), a self-consistent forward modelling code, with a f factor of 0.6 (implying close to zero albedo and zero day-to-night recirculation), a metallicity of 0.1x solar, and a

C/O ratio of 0.3. The HELIOS model predicts temperatures colder than our retrieval results at low pressures, where our retrievals are insensitive, but the temperatures are in agreement at the photospheric pressures of ~ 30 – 1000 mbar.

The temperature jacobians J_T in the second panel of [Figure 2](#) are computed by numerically deriving the spectrum F_p with respect to the

temperature T , similarly to the approach outlined by [Eyre et al. \(1993\)](#) and [Garand et al. \(2001\)](#). This method, described in Equation 2, allows to assess how sensitive the spectral data is to small variations of temperature along the vertical pressure structure, i.e. what layers are being probed.

$$J_T = \frac{f_p(T + \delta T) - f_p(T - \delta T)}{2 \cdot \delta T} \quad (2)$$

The abundance profiles are shown in the third panel of Figure 2. Similarly, one can induce small variation of the abundance of specific molecule X and compute the resulting spectral fluctuations to characterise sensitivity. In this case, it is more intuitive to perform a log-derivative of the eclipse depth like in Equation 3.

$$J_X = \frac{f_p(n_X + \delta n_X) - f_p(n_X - \delta n_X)}{2 \cdot \delta n_X} \cdot n_X \quad (3)$$

For the three subplots on the far right panel of Figure 2, we preferred a base-10 logarithm to match the x-axis graduation on the left panel.

The equilibrium chemistry model yields a metallicity of $[M/H] = -0.91_{-0.16}^{+0.24}$ (ie. about 0.1 – 0.2 times solar) and a carbon-to-oxygen ratio of $C/O = 0.36_{-0.09}^{+0.10}$. The free retrieval yields molecular abundances of $\log_{10}(n_{H_2O}) = -4.26_{-0.10}^{+0.14}$ for water and $\log_{10}(n_{CO}) = -4.58_{-0.24}^{+0.27}$ for carbon monoxide. It also puts an upper limit on the carbon dioxide abundance $\log_{10}(n_{CO_2}) < -7.50$ at 3σ . These results compare well to the abundances estimated through equilibrium chemistry.

The [Mansfield et al. \(2022\)](#) HST WFC3 data seemed to fall within the continuity of the spectrum, so we attempted a joint analysis as shown on Figure 3. These retrievals reevaluate metallicity and C/O ratio to higher values, $[M/H] = -0.06_{-0.16}^{+0.13}$ and $C/O = 0.60_{-0.05}^{+0.04}$. However, the models do not fit the data very well. While the reduced χ^2 (1.17, compared to the JWST-only reduced $\chi^2 = 0.78$) is not bad per se, the fit to

the WFC3 data is systematically wrong by eye. The shape of the HST spectral data cannot be reproduced by our models, and this can't be fixed by adding a simple offset. Whether this is due to poor data quality, aerosols in the planet's atmosphere, or a combination is unclear, and our attempts at accounting for these in the retrievals were unsuccessful. Given the agreement between the JWST and high-resolution results, we suspect that the HST data are not fully reliable.

The JWST-only results confirm the sub-solar metallicity inferred by [Line et al. \(2021\)](#) using high-resolution spectroscopy with IGRINS, agreeing at $\sim 1\sigma$. The C/O ratios agree at about 1.8σ , as our retrievals favour a sub-solar value. Figure 3 shows the concordance of our spectrum and models with other datasets, namely the Spitzer and HST WFC3 datapoints as well as the [Line et al. \(2021\)](#) generated spectrum from the HRS results. The PLATON retrieval results were confirmed using a retrieval with a GPU-accelerated version of CHIMERA ([Line et al. 2013b](#); [Brogi & Line 2019](#)), adapted for equilibrium chemistry by using GGChem ([Woitke et al. 2018](#)), which yielded a metallicity of $[M/H] = -0.85_{-0.12}^{+0.20}$ and a carbon-to-oxygen ratio of $C/O = 0.32_{-0.09}^{+0.14}$.

4. COMPARATIVE PLANETOLOGY

Here we compare our spectrum of WASP-77Ab to the JWST spectrum of HD 149026b that was recently presented by [Bean et al. \(2023\)](#). These planets have similar equilibrium temperatures (1705 vs. 1634 K, respectively) and now both have high-quality thermal emission spectra from 2.8 – 5.0 μm . To put the spectra on the same scale, we converted the measured secondary eclipse depths (F_p/F_s) to brightness temperatures. We used stellar spectra computed with HELIOS ([Malik et al. 2017a, 2019a](#)) for the conversion. The stellar parameters used are $T_{\text{eff}} = 5525\text{K}$, $\log g = 4.44$, and $[M/H] = 0.0$ for WASP-77A ([Reggiani et al.](#)

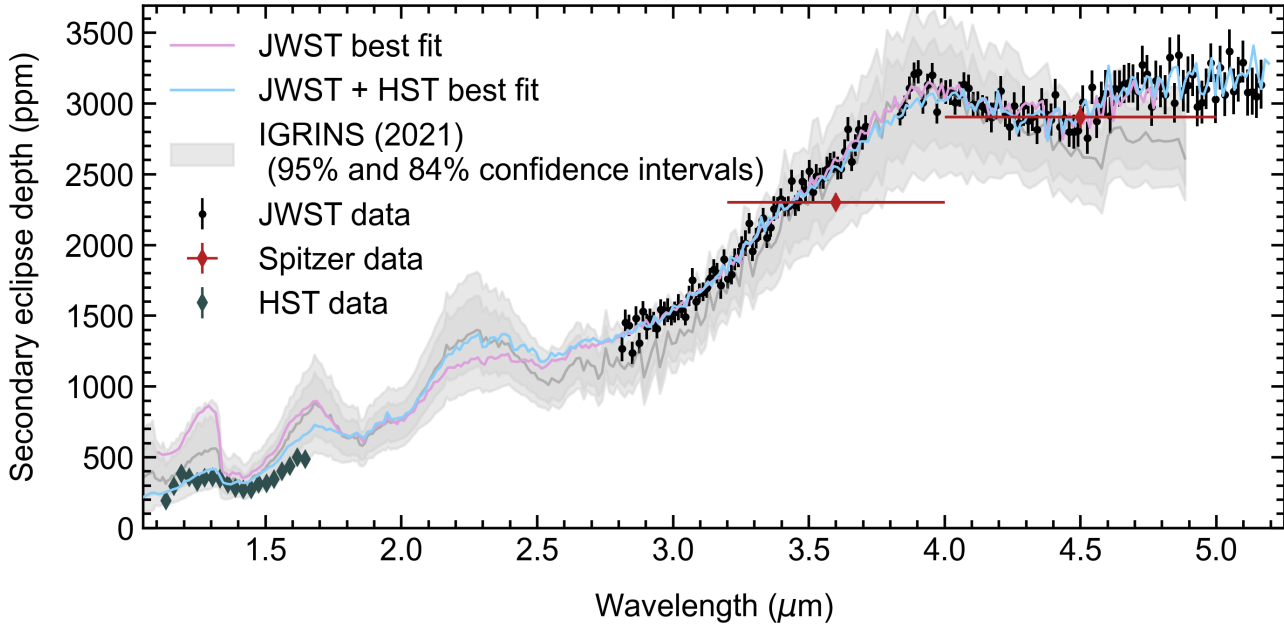


Figure 3. Concordance of our JWST NIRSpec data and retrieval results with other data sets (Spitzer, HST WFC3) and the reconstructed spectrum from high-resolution spectroscopy results with IGRINS.

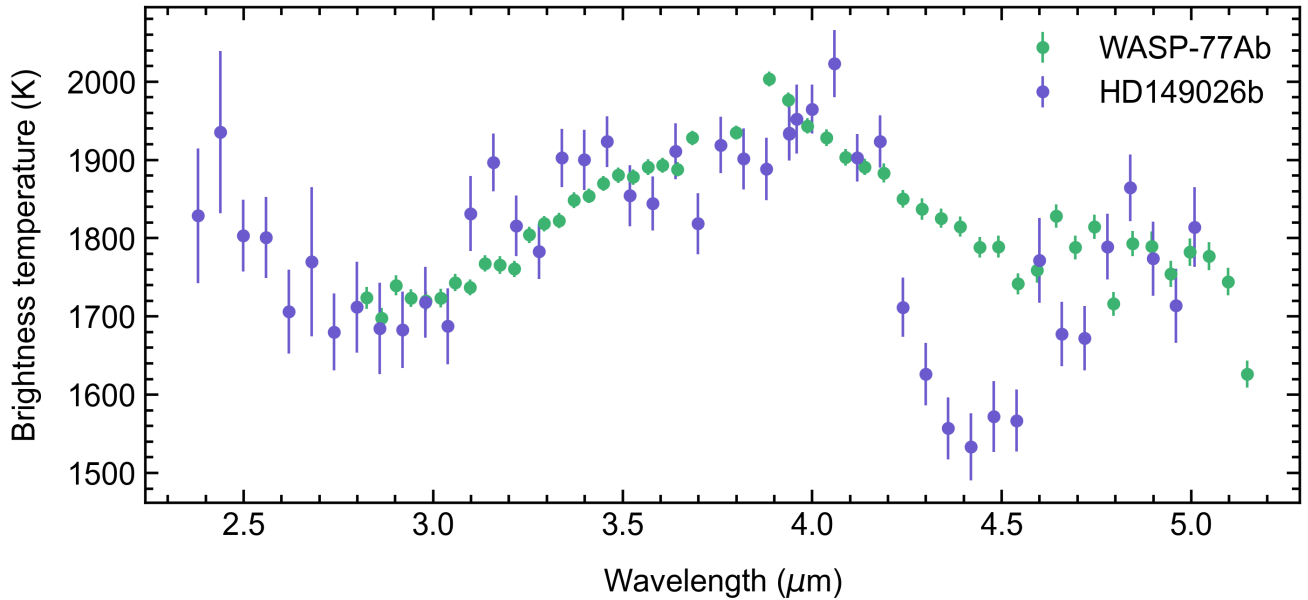


Figure 4. Planetary brightness temperatures of HD 149026b (purple points, [Bean et al. 2023](#)) and WASP-77Ab (green points) from JWST thermal emission spectra. The spectrum of HD 149026b exhibits strong absorption due to CO_2 that is absent from the spectrum of WASP-77Ab.

2022), and $T_{\text{eff}} = 6085\text{K}$, $\log g = 4.19$, and $[M/H] = 0.25$ for HD 149026 (Bean et al. 2023). Then a blackbody function was fitted to the planet flux measurement in order to determine the brightness temperature at each wavelength. These temperatures are then binned by an arbitrary factor of three for clarity and shown in Figure 4 for both planets.

Aside from the astounding S/N ratio for WASP-77Ab, it is remarkable how similar both planets’ brightness temperature spectra are across the wavelength range that is dominated by H₂O and CO opacity. In contrast, their atmospheric chemistry is visibly different as shown by the strong CO₂ feature at 4.4 μm in HD 149026b. CO₂ is an excellent metallicity indicator for hot, giant planets (Lodders & Fegley 2002; Zahnle et al. 2009; Moses et al. 2013). Therefore, it is easily apparent that the metallicities of these two objects are very different. This illustrates the rich diversity of exoplanetary atmospheres, which was forecasted from HST WFC3 results leading up to JWST by Mansfield et al. (2021).

Is the diversity of exoplanet metallicity determined by a small number of processes that relate directly to some specific aspect of formation, or is it more stochastic? Line et al. (2021) constructed a solar system trend line of metallicity enrichment versus mass, and plotted WASP77Ab well below that line. Our metallicity result is lower but consistent at the $\sim 1\sigma$ level. They interpret the low metallicity of the atmosphere and solar C/O value in terms of a planet with most of the metals in a discrete core, and a lack of both planetesimal bombardment and significant radial migration in the disk. Our C/O value falls below the solar value, and would imply instead a radial migration that accumulates O-rich and C-poor material based on the Line et al. (2021) systematics. HD 149026b, on the other hand, plots well above the solar system trend line in metallicity, has an enriched

C/O value, and a massively extended (diffuse) core (Bean et al. 2023). If the latter is the result of a giant collision (Ikoma et al. 2006), then these two objects represent outcomes of very different planetary accretion processes. This might argue that the diversity of giant planet atmospheres is reflective of a diversity in planetary formation, and stochastic events such as giant collisions are important.

Complicating this picture is the question of whether the atmospheric compositions of planets should be interpreted in the context of an absolute scale (in this paper we use the solar abundance pattern from Asplund et al. 2009) or relative to the abundances of each of their host stars. For example, Kolecki & Wang (2022), Polanski et al. (2022), and Reggiani et al. (2022) have argued for the latter approach and have presented stellar abundances for WASP-77Ab (all three papers) and HD 149026b (just the first two papers). WASP-77A is consistently found by all three studies to have solar to potentially slightly sub-solar iron abundance. However, Reggiani et al. (2022) suggested that carbon and oxygen, which are what we are measuring in the planets and calling metallicity, were together about 2x solar. On the other hand, Kolecki & Wang (2022) and Polanski et al. (2022) found the carbon and oxygen abundances more in line with the iron abundance.

For HD 149026, all authors plus Brewer et al. (2016) and Brewer & Fischer (2016) consistently find that the iron, carbon, and oxygen are roughly 2x solar, with a slight preference for super-solar C/O from Kolecki & Wang (2022). If the atmospheric metallicity inferred for HD 149026b is “corrected” for the host star metallicity then its atmospheric metal enhancement is reduced to $\sim 100\text{x}$, which is still well above the solar system trend line (Kreidberg et al. 2014; Line et al. 2021; Bean et al. 2023) and significantly different than that of WASP-77Ab.

5. CONCLUSION

Hot Jupiters present an opportunity to measure the atmospheric abundances of both carbon- and oxygen-bearing species, which is extremely challenging for the solar system giants due to their cold temperatures (Guillot et al. 2022). We have presented the third thermal emission spectrum of a hot Jupiter from JWST, following WASP-18b (Coulombe et al. 2023) and HD 149026b (Bean et al. 2023). Our spectrum of WASP-77Ab shows absorption from H₂O and CO, but strikingly no CO₂. Modeling the data indicates a strongly sub-solar metallicity for the planet’s atmosphere, which is in excellent agreement with the result from the IGRINS ground-based HRS presented by (Line et al. 2021). The agreement sets the stage for a combined analysis of these state-of-the-art data sets that may yield further insight into the properties of WASP-77Ab’s atmosphere (P. Smith in preparation).

Early results from JWST show conclusively that hot Jupiter atmospheres have diverse compositions. We have already seen that metallicities can range from sub-solar (WASP-77Ab), to solar (WASP-18b: Coulombe et al. 2023), to modestly ($\sim 10x$) super-solar (WASP-39b: JWST Transiting Exoplanet Community Early Release Science Team et al. 2023; Rustamkulov et al. 2023; Feinstein et al. 2023; Alderson et al. 2023; Ahrer et al. 2023; Tsai et al. 2022), to even very ($\sim 200x$) super-solar (HD149026b: Bean et al. 2023). The diversity of giant planet at-

mosphere compositions that has emerged from early JWST results implies that our search for statistical trends like the mass-metallicity relationship (e.g., Fortney et al. 2013; Kreidberg et al. 2014) and the bulk-atmosphere metallicity correlation (Bean et al. 2023) will require dozens of objects, or more.

We thank Eugenio Schisano and Ji Wang for discussions about planet host star abundances. This work is based on observations made with the NASA/ESA/CSA James Webb Space Telescope. The data were obtained from the Mikulski Archive for Space Telescopes at the Space Telescope Science Institute, which is operated by the Association of Universities for Research in Astronomy, Inc., under NASA contract NAS 5-03127 for JWST. The specific observations analyzed can be accessed via DOI: [10.17909/3fmp-zj55](https://doi.org/10.17909/3fmp-zj55). JL was supported by NASA grant NNX17AL71A, and was in residence at the Dominican House of Studies, Washington DC, as the McDonald Agape Visiting Scholar, during the data analysis and preparation of the manuscript. MZ acknowledges support from the 51 Pegasi b Fellowship funded by the Heising-Simons Foundation.

Facilities: JWST (STScI)

Software: Eureka! (Bell et al. 2022), PLATON (Zhang et al. 2020), HELIOS (Malik et al. 2017a, 2019a), HELIOS-K (Grimm et al. 2021), CHIMERA (Line et al. 2013b; Brogi & Line 2019)

APPENDIX

A. SPECTRAL DATA

Wavelength (μm)	Ecl. depth (ppm)	Err., low (ppm)	Err., high (ppm)	Best fit (ppm)	No H ₂ O (ppm)	No CO (ppm)	No H ₂ S (ppm)	No CO ₂ (ppm)
2.808 - 2.814	1267	89	88	1394	2059	1394	1398	1394
2.821 - 2.827	1450	85	91	1372	2090	1372	1376	1372
2.834 - 2.840	1433	77	75	1358	2126	1358	1359	1358

Wavelength (μm)	Ecl. depth (ppm)	Err., low (ppm)	Err., high (ppm)	Best fit (ppm)	No H ₂ O (ppm)	No CO (ppm)	No H ₂ S (ppm)	No CO ₂ (ppm)
2.847 - 2.853	1237	79	80	1396	2154	1396	1398	1396
2.860 - 2.866	1481	80	85	1404	2170	1404	1406	1404
2.873 - 2.879	1306	70	73	1462	2213	1462	1465	1462
2.886 - 2.892	1529	78	74	1393	2232	1393	1394	1393
2.899 - 2.905	1420	88	94	1447	2269	1447	1448	1447
2.912 - 2.918	1477	75	74	1449	2282	1449	1450	1449
2.925 - 2.931	1457	70	70	1471	2326	1471	1472	1471
2.938 - 2.944	1407	67	66	1468	2351	1468	1469	1468
2.951 - 2.957	1542	72	72	1483	2363	1483	1484	1483
2.964 - 2.970	1513	83	85	1488	2392	1488	1489	1488
2.977 - 2.983	1537	82	85	1538	2417	1538	1539	1538
2.990 - 2.996	1499	66	67	1527	2446	1527	1527	1527
3.003 - 3.009	1524	71	74	1517	2467	1517	1518	1517
3.016 - 3.022	1559	91	92	1588	2495	1588	1589	1588
3.029 - 3.035	1546	62	64	1590	2540	1590	1590	1590
3.042 - 3.048	1490	57	61	1545	2539	1545	1545	1545
3.055 - 3.061	1637	70	75	1666	2555	1666	1666	1666
3.068 - 3.074	1752	83	85	1594	2578	1594	1594	1594
3.081 - 3.087	1600	65	67	1664	2612	1664	1664	1664
3.094 - 3.100	1660	67	67	1657	2629	1657	1657	1657
3.107 - 3.113	1667	63	67	1690	2672	1690	1690	1690
3.120 - 3.126	1694	67	70	1722	2660	1722	1723	1722
3.133 - 3.139	1763	70	74	1745	2682	1745	1745	1745
3.146 - 3.152	1825	70	72	1778	2723	1778	1778	1778
3.159 - 3.165	1800	71	73	1832	2726	1832	1832	1832
3.172 - 3.178	1715	95	90	1770	2755	1770	1770	1770
3.185 - 3.191	1898	68	70	1838	2754	1838	1838	1838
3.198 - 3.204	1761	68	68	1768	2807	1768	1769	1768
3.211 - 3.217	1791	69	69	1948	2813	1948	1948	1948
3.224 - 3.230	1900	78	76	1853	2812	1853	1853	1853
3.237 - 3.243	1907	62	69	1876	2842	1876	1876	1876
3.250 - 3.256	1993	65	67	1964	2844	1964	1965	1964
3.263 - 3.269	2012	89	91	1992	2860	1992	1993	1992
3.276 - 3.282	2152	73	74	1948	2884	1948	1948	1948
3.289 - 3.295	1956	69	73	1998	2952	1998	1998	1998
3.302 - 3.309	2048	72	71	2047	2917	2047	2048	2047
3.316 - 3.322	2112	76	75	2158	3008	2158	2159	2158
3.329 - 3.335	2190	72	73	2193	2926	2193	2194	2193
3.342 - 3.348	2052	72	74	2095	2944	2095	2096	2095
3.355 - 3.361	2123	66	67	2190	2956	2190	2191	2190

Wavelength (μm)	Ecl. depth (ppm)	Err., low (ppm)	Err., high (ppm)	Best fit (ppm)	No H ₂ O (ppm)	No CO (ppm)	No H ₂ S (ppm)	No CO ₂ (ppm)
3.368 - 3.374	2255	84	88	2181	3004	2181	2182	2181
3.381 - 3.387	2261	72	75	2191	2999	2191	2192	2191
3.394 - 3.400	2323	76	76	2364	3147	2364	2366	2364
3.407 - 3.413	2267	64	68	2256	3045	2256	2258	2256
3.420 - 3.426	2270	67	73	2292	3052	2292	2294	2292
3.433 - 3.439	2454	78	79	2345	3057	2345	2349	2345
3.446 - 3.452	2278	73	71	2380	3077	2380	2383	2380
3.459 - 3.465	2312	72	70	2346	3072	2346	2350	2346
3.472 - 3.478	2449	78	78	2354	3083	2354	2360	2354
3.485 - 3.491	2386	78	73	2418	3088	2418	2429	2418
3.498 - 3.504	2522	78	78	2419	3104	2419	2427	2419
3.511 - 3.517	2374	67	77	2447	3105	2447	2465	2447
3.524 - 3.530	2486	88	86	2359	3118	2359	2371	2359
3.537 - 3.543	2471	73	75	2472	3135	2472	2489	2472
3.550 - 3.556	2471	75	78	2489	3136	2489	2502	2489
3.563 - 3.569	2534	83	87	2523	3151	2523	2538	2523
3.576 - 3.582	2575	71	74	2530	3149	2530	2552	2530
3.589 - 3.595	2586	75	74	2638	3152	2638	2666	2638
3.602 - 3.608	2546	84	79	2647	3156	2647	2669	2647
3.615 - 3.621	2537	69	71	2646	3162	2646	2672	2646
3.628 - 3.634	2659	77	86	2691	3194	2691	2719	2691
3.641 - 3.647	2820	88	85	2735	3217	2735	2756	2735
3.654 - 3.660	2589	65	70	2708	3236	2708	2734	2708
3.667 - 3.673	2703	77	78	2771	3233	2771	2794	2771
3.680 - 3.686	2814	67	68	2782	3263	2782	2810	2782
3.693 - 3.699	2752	80	80	2809	3274	2809	2834	2809
3.706 - 3.712	2838	85	79	2774	3234	2774	2805	2774
3.831 - 3.839	2914	69	73	2983	3365	2983	3003	2983
3.848 - 3.856	2983	71	74	3027	3366	3027	3050	3027
3.865 - 3.873	3109	81	82	3021	3394	3021	3041	3021
3.882 - 3.890	3208	84	82	3135	3406	3135	3160	3135
3.899 - 3.907	3220	78	85	3114	3405	3114	3134	3114
3.915 - 3.923	3005	77	79	3111	3409	3111	3135	3111
3.932 - 3.940	3131	76	80	3152	3426	3152	3173	3152
3.949 - 3.957	3200	86	86	3130	3465	3130	3149	3130
3.966 - 3.974	2939	81	85	3068	3436	3068	3089	3068
3.983 - 3.991	3101	72	77	3120	3482	3120	3138	3120
4.000 - 4.008	3077	82	86	3045	3463	3045	3062	3045
4.016 - 4.024	3077	88	92	3096	3477	3096	3114	3096
4.033 - 4.041	3007	85	94	3082	3491	3082	3095	3082

Wavelength (μm)	Ecl. depth (ppm)	Err., low (ppm)	Err., high (ppm)	Best fit (ppm)	No H ₂ O (ppm)	No CO (ppm)	No H ₂ S (ppm)	No CO ₂ (ppm)
4.050 - 4.058	3061	83	92	3078	3526	3078	3094	3078
4.067 - 4.075	3133	92	88	3146	3616	3146	3158	3146
4.084 - 4.092	3107	97	98	2936	3540	2936	2948	2936
4.100 - 4.108	2993	88	89	3023	3537	3023	3037	3023
4.117 - 4.125	2992	90	93	3010	3536	3010	3019	3010
4.134 - 4.142	2975	79	82	3032	3578	3032	3040	3032
4.151 - 4.159	2955	87	92	2989	3563	2989	2996	2989
4.168 - 4.176	2900	107	163	2972	3516	2967	2973	2971
4.185 - 4.193	2987	98	97	2992	3600	2992	3000	2993
4.201 - 4.209	3088	100	183	3029	3663	3045	3079	3057
4.218 - 4.226	2928	94	92	2998	3583	2998	3004	3004
4.235 - 4.243	2835	95	98	2938	3590	2938	2942	2945
4.252 - 4.260	2983	101	99	2947	3598	2941	2956	2952
4.269 - 4.277	2860	95	95	2903	3602	2903	2907	2913
4.286 - 4.294	2983	146	107	2992	3652	2932	2990	3075
4.302 - 4.310	2876	108	183	3031	3604	3062	3029	3026
4.319 - 4.327	2905	109	116	3059	3569	3156	3067	3006
4.336 - 4.344	2816	106	110	3035	3496	3163	3090	3018
4.353 - 4.361	3009	101	137	3005	3374	3114	3031	3000
4.370 - 4.378	2925	112	155	2733	2813	3135	2767	2777
4.387 - 4.395	2885	113	129	2900	3100	3160	2994	2981
4.403 - 4.411	3061	109	167	2925	3017	3348	2989	2913
4.420 - 4.428	2834	103	136	2914	3294	3170	2955	2927
4.437 - 4.445	2898	114	173	2849	3105	3060	2822	2871
4.454 - 4.462	2799	108	185	2915	3132	3127	2973	2965
4.471 - 4.479	2800	120	182	2771	2814	3216	2793	2769
4.487 - 4.495	2807	119	182	2832	2924	3174	2830	2860
4.504 - 4.512	3008	123	115	2775	2995	3109	2768	2705
4.521 - 4.529	2757	117	124	3026	3219	3338	3032	3023
4.538 - 4.546	3115	115	169	2852	2985	3367	2885	2850
4.555 - 4.563	2875	118	197	3007	3274	3397	3067	3062
4.572 - 4.580	3025	123	128	2857	3039	3299	2840	2806
4.588 - 4.596	3071	168	184	2977	3153	3314	2965	2997
4.605 - 4.613	2914	129	163	3249	3461	3604	3258	3223
4.622 - 4.630	3105	125	185	2917	3017	3360	2994	2973
4.639 - 4.647	3101	120	173	3002	3170	3343	3087	3093
4.656 - 4.664	3137	133	161	3113	3425	3279	3197	3100
4.673 - 4.681	3146	142	113	2990	3317	3151	2987	2949
4.689 - 4.697	3143	133	164	3217	3548	3359	3292	3279
4.706 - 4.714	3086	130	144	3075	3402	3122	3038	3035

Wavelength (μm)	Ecl. depth (ppm)	Err., low (ppm)	Err., high (ppm)	Best fit (ppm)	No H ₂ O (ppm)	No CO (ppm)	No H ₂ S (ppm)	No CO ₂ (ppm)
4.723 - 4.731	3273	135	175	3052	3564	3111	3043	3036
4.740 - 4.748	3205	134	197	3092	3389	3375	3098	3027
4.757 - 4.765	2978	137	144	3110	3453	3373	3151	3139
4.773 - 4.781	3160	136	100	3115	3524	3298	3165	3145
4.790 - 4.798	3121	147	107	3076	3407	3253	3029	3015
4.807 - 4.815	3063	136	155	2967	3191	3252	2943	2963
4.824 - 4.832	3326	148	196	3261	3608	3451	3261	3227
4.841 - 4.849	3004	142	122	3095	3425	3291	3057	3086
4.858 - 4.866	3341	156	147	3198	3547	3380	3157	3111
4.874 - 4.882	3090	149	115	3113	3497	3220	3106	3125
4.891 - 4.899	3128	193	250	3045	3371	3142	3041	3035
4.908 - 4.916	3203	157	106	3160	3420	3321	3104	3147
4.925 - 4.933	2978	143	100	3097	3362	3283	3034	3013
4.942 - 4.950	3005	144	108	2988	3254	3167	2960	2971
4.959 - 4.967	3100	148	139	3001	3173	3277	3038	3011
4.975 - 4.983	3286	139	162	3235	3565	3357	3291	3207
4.992 - 5.000	3028	167	188	3112	3522	3258	3141	3120
5.009 - 5.017	3252	153	191	3154	3300	3201	3148	3125
5.026 - 5.034	3061	156	106	3006	3273	3100	3093	3033
5.043 - 5.051	3368	155	194	3219	3876	3217	3277	3255
5.060 - 5.068	3085	169	164	3102	3609	3214	3117	3175
5.076 - 5.084	3170	156	108	3112	3688	3154	3122	3124
5.093 - 5.101	3290	144	111	3226	3861	3273	3250	3273
5.110 - 5.118	3077	166	157	3195	3880	3259	3181	3164
5.127 - 5.135	3082	162	118	3205	3808	3295	3214	3232
5.144 - 5.152	3050	152	196	3069	3339	3150	3024	3068
5.160 - 5.168	3130	160	150	3058	3345	3131	3039	3004

Table 2. Summary of the spectral data shown on Figure 1.

REFERENCES

- Ahrer, E.-M., Stevenson, K. B., Mansfield, M., et al. 2023, *Nature*, 614, 653, doi: [10.1038/s41586-022-05590-4](https://doi.org/10.1038/s41586-022-05590-4)
- Alderson, L., Wakeford, H. R., Alam, M. K., et al. 2023, *Nature*, 614, 664, doi: [10.1038/s41586-022-05591-3](https://doi.org/10.1038/s41586-022-05591-3)
- Asplund, M., Grevesse, N., Sauval, A. J., & Scott, P. 2009, *ARA&A*, 47, 481, doi: [10.1146/annurev.astro.46.060407.145222](https://doi.org/10.1146/annurev.astro.46.060407.145222)
- Bean, J. L., Xue, Q., August, P. C., et al. 2023, *Nature*, 618, 43, doi: [10.1038/s41586-023-05984-y](https://doi.org/10.1038/s41586-023-05984-y)
- Bell, T. J., Ahrer, E.-M., Brande, J., et al. 2022, *Journal of Open Source Software*, 7, 4503, doi: [10.21105/joss.04503](https://doi.org/10.21105/joss.04503)

- Benneke, B. 2015, Strict Upper Limits on the Carbon-to-Oxygen Ratios of Eight Hot Jupiters from Self-Consistent Atmospheric Retrieval, arXiv, doi: [10.48550/ARXIV.1504.07655](https://doi.org/10.48550/ARXIV.1504.07655)
- Birkmann, S. M., Ferruit, P., Giardino, G., et al. 2022, *A&A*, 661, A83
- Bitsch, B., Schneider, A. D., & Kreidberg, L. 2022, *A&A*, 665, A138, doi: [10.1051/0004-6361/202243345](https://doi.org/10.1051/0004-6361/202243345)
- Brewer, J. M., & Fischer, D. A. 2016, *ApJ*, 831, 20, doi: [10.3847/0004-637X/831/1/20](https://doi.org/10.3847/0004-637X/831/1/20)
- Brewer, J. M., Fischer, D. A., Valenti, J. A., & Piskunov, N. 2016, *ApJS*, 225, 32, doi: [10.3847/0067-0049/225/2/32](https://doi.org/10.3847/0067-0049/225/2/32)
- Brogi, M., & Line, M. R. 2019, *AJ*, 157, 114, doi: [10.3847/1538-3881/aaffd3](https://doi.org/10.3847/1538-3881/aaffd3)
- Bushouse, H., Eisenhamer, J., Dencheva, N., et al. 2023, Zenodo, doi: [10.5281/zenodo.7692609](https://doi.org/10.5281/zenodo.7692609)
- Cortés-Zuleta, P., Rojo, P., Wang, S., et al. 2020, *A&A*, 636, A98, doi: [10.1051/0004-6361/201936279](https://doi.org/10.1051/0004-6361/201936279)
- Coulombe, L.-P., Benneke, B., Challener, R., et al. 2023, arXiv e-prints, arXiv:2301.08192, doi: [10.48550/arXiv.2301.08192](https://doi.org/10.48550/arXiv.2301.08192)
- Eyre, J. R., Kelly, G. A., McNally, A. P., Andersson, E., & Persson, A. 1993, *Quarterly Journal of the Royal Meteorological Society*, 119, 1427, doi: <https://doi.org/10.1002/qj.49711951411>
- Feinstein, A. D., Radica, M., Welbanks, L., et al. 2023, *Nature*, 614, 670, doi: [10.1038/s41586-022-05674-1](https://doi.org/10.1038/s41586-022-05674-1)
- Fortney, J. J., Dawson, R. I., & Komacek, T. D. 2021, *Journal of Geophysical Research: Planets*, 126, doi: [10.1029/2020je006629](https://doi.org/10.1029/2020je006629)
- Fortney, J. J., Mordasini, C., Nettelmann, N., et al. 2013, *The Astrophysical Journal*, 775, 80, doi: [10.1088/0004-637X/775/1/80](https://doi.org/10.1088/0004-637X/775/1/80)
- Garand, L., Turner, D. S., Larocque, M., et al. 2001, *Journal of Geophysical Research: Atmospheres*, 106, 24017, doi: <https://doi.org/10.1029/2000JD000184>
- Greene, T. P., Line, M. R., Montero, C., et al. 2016, *ApJ*, 817, 17
- Grimm, S. L., Malik, M., Kitzmann, D., et al. 2021, *ApJS*, 253, 30, doi: [10.3847/1538-4365/abd773](https://doi.org/10.3847/1538-4365/abd773)
- Guillot, T. 2010, *Astronomy and Astrophysics*, 520, A27, doi: [10.1051/0004-6361/200913396](https://doi.org/10.1051/0004-6361/200913396)
- Guillot, T., Fletcher, L. N., Helled, R., et al. 2022, arXiv e-prints, arXiv:2205.04100, doi: [10.48550/arXiv.2205.04100](https://doi.org/10.48550/arXiv.2205.04100)
- Ikoma, M., Guillot, T., Genda, H., Tanigawa, T., & Ida, S. 2006, *The Astrophysical Journal*, 650, 1150, doi: [10.1086/507088](https://doi.org/10.1086/507088)
- Ivshina, E. S., & Winn, J. N. 2022, *ApJS*, 259, 62, doi: [10.3847/1538-4365/ac545b](https://doi.org/10.3847/1538-4365/ac545b)
- JWST Transiting Exoplanet Community Early Release Science Team, Ahrer, E.-M., Alderson, L., et al. 2023, *Nature*, 614, 649, doi: [10.1038/s41586-022-05269-w](https://doi.org/10.1038/s41586-022-05269-w)
- Kempton, E. M.-R., Bean, J. L., Louie, D. R., et al. 2018, *Publications of the Astronomical Society of the Pacific*, 130, 114401, doi: [10.1088/1538-3873/aadf6f](https://doi.org/10.1088/1538-3873/aadf6f)
- Kokori, A., Tsiaras, A., Edwards, B., et al. 2022, *ApJS*, 258, 40, doi: [10.3847/1538-4365/ac3a10](https://doi.org/10.3847/1538-4365/ac3a10)
- Kolecki, J. R., & Wang, J. 2022, *AJ*, 164, 87, doi: [10.3847/1538-3881/ac7de3](https://doi.org/10.3847/1538-3881/ac7de3)
- Kreidberg, L., Bean, J. L., Désert, J.-M., et al. 2014, *ApJL*, 793, L27, doi: [10.1088/2041-8205/793/2/L27](https://doi.org/10.1088/2041-8205/793/2/L27)
- Kreidberg, L., Line, M. R., Bean, J. L., et al. 2015, A Detection of Water in the Transmission Spectrum of the Hot Jupiter WASP-12b and Implications for its Atmospheric Composition, arXiv, doi: [10.48550/ARXIV.1504.05586](https://doi.org/10.48550/ARXIV.1504.05586)
- Line, M. R., Wolf, A. S., Zhang, X., et al. 2013a, *The Astrophysical Journal*, 775, 137
- . 2013b, *The Astrophysical Journal*, 775, 137, doi: [10.1088/0004-637x/775/2/137](https://doi.org/10.1088/0004-637x/775/2/137)
- Line, M. R., Brogi, M., Bean, J. L., et al. 2021, *Nature*, 598, 580
- Lodders, K., & Fegley, B. 2002, *Icarus*, 155, 393, doi: [10.1006/icar.2001.6740](https://doi.org/10.1006/icar.2001.6740)
- Lustig-Yaeger, J., Fu, G., May, E. M., et al. 2023, arXiv e-prints, arXiv:2301.04191, doi: [10.48550/arXiv.2301.04191](https://doi.org/10.48550/arXiv.2301.04191)
- Madhusudhan, N. 2012, *The Astrophysical Journal*, 758, 36, doi: [10.1088/0004-637X/758/1/36](https://doi.org/10.1088/0004-637X/758/1/36)
- . 2019, *Annual Review of Astronomy and Astrophysics*, 57, 617, doi: [10.1146/annurev-astro-081817-051846](https://doi.org/10.1146/annurev-astro-081817-051846)
- Madhusudhan, N., & Seager, S. 2009, *The Astrophysical Journal*, 707, 24, doi: [10.1088/0004-637x/707/1/24](https://doi.org/10.1088/0004-637x/707/1/24)
- Malik, M., Kitzmann, D., Mendonça, J. M., et al. 2019a, *AJ*, 157, 170

- . 2019b, *AJ*, 157, 170,
doi: [10.3847/1538-3881/ab1084](https://doi.org/10.3847/1538-3881/ab1084)
- Malik, M., Grosheintz, L., Mendonça, J. M., et al. 2017a, *AJ*, 153, 56
- . 2017b, *AJ*, 153, 56,
doi: [10.3847/1538-3881/153/2/56](https://doi.org/10.3847/1538-3881/153/2/56)
- Mansfield, M., Line, M. R., Bean, J. L., et al. 2021, *Nature Astronomy*, 5, 1224,
doi: [10.1038/s41550-021-01455-4](https://doi.org/10.1038/s41550-021-01455-4)
- Mansfield, M., Wisner, L., Stevenson, K. B., et al. 2022, *The Astronomical Journal*, 163, 261
- Maxted, P. F. L., Anderson, D. R., Collier Cameron, A., et al. 2013, *PASP*, 125, 48,
doi: [10.1086/669231](https://doi.org/10.1086/669231)
- Mikal-Evans, T., Sing, D. K., Dong, J., et al. 2023, *ApJL*, 943, L17, doi: [10.3847/2041-8213/acb049](https://doi.org/10.3847/2041-8213/acb049)
- Moran, S. E., Stevenson, K. B., Sing, D. K., et al. 2023, *ApJL*, 948, L11,
doi: [10.3847/2041-8213/accb9c](https://doi.org/10.3847/2041-8213/accb9c)
- Mordasini, C., van Boekel, R., Mollière, P., Henning, T., & Benneke, B. 2016, *The Astrophysical Journal*, 832, 41,
doi: [10.3847/0004-637X/832/1/41](https://doi.org/10.3847/0004-637X/832/1/41)
- Moses, J. I., Line, M. R., Visscher, C., et al. 2013, *ApJ*, 777, 34, doi: [10.1088/0004-637X/777/1/34](https://doi.org/10.1088/0004-637X/777/1/34)
- Polanski, A. S., Crossfield, I. J. M., Howard, A. W., Isaacson, H., & Rice, M. 2022, *Research Notes of the American Astronomical Society*, 6, 155, doi: [10.3847/2515-5172/ac8676](https://doi.org/10.3847/2515-5172/ac8676)
- Pollack, J. B., Hubickyj, O., Bodenheimer, P., et al. 1996, *Icarus*, 124, 62,
doi: [10.1006/icar.1996.0190](https://doi.org/10.1006/icar.1996.0190)
- Reggiani, H., Schlaufman, K. C., Healy, B. F., Lothringer, J. D., & Sing, D. K. 2022, *The Astronomical Journal*, 163, 159,
doi: [10.3847/1538-3881/ac4d9f](https://doi.org/10.3847/1538-3881/ac4d9f)
- Rustamkulov, Z., Sing, D. K., Mukherjee, S., et al. 2023, *Nature*, 614, 659,
doi: [10.1038/s41586-022-05677-y](https://doi.org/10.1038/s41586-022-05677-y)
- Taylor, J., Parmentier, V., Irwin, P. G. J., et al. 2020, *Monthly Notices of the Royal Astronomical Society*, 493, 4342,
doi: [10.1093/mnras/staa552](https://doi.org/10.1093/mnras/staa552)
- Tsai, S.-M., Lee, E. K. H., Powell, D., et al. 2022, arXiv e-prints, arXiv:2211.10490,
doi: [10.48550/arXiv.2211.10490](https://doi.org/10.48550/arXiv.2211.10490)
- Venturini, J., Alibert, Y., & Benz, W. 2016, *Astronomy & Astrophysics*, 596, A90,
doi: [10.1051/0004-6361/201628828](https://doi.org/10.1051/0004-6361/201628828)
- Woitke, P., Helling, C., Hunter, G. H., et al. 2018, *Astronomy & Astrophysics*, 614, A1,
doi: [10.1051/0004-6361/201732193](https://doi.org/10.1051/0004-6361/201732193)
- Zahnle, K., Marley, M. S., Freedman, R. S., Lodders, K., & Fortney, J. J. 2009, *ApJL*, 701, L20, doi: [10.1088/0004-637X/701/1/L20](https://doi.org/10.1088/0004-637X/701/1/L20)
- Zhang, M., Chachan, Y., Kempton, E. M. R., & Knutson, H. A. 2019, *PASP*, 131, 034501,
doi: [10.1088/1538-3873/aaf5ad](https://doi.org/10.1088/1538-3873/aaf5ad)
- Zhang, M., Chachan, Y., Kempton, E. M.-R., Knutson, H. A., & Chang, W. H. 2020, *The Astrophysical Journal*, 899, 27,
doi: [10.3847/1538-4357/aba1e6](https://doi.org/10.3847/1538-4357/aba1e6)